Reef Flat Flow Dynamics for a Nearly Closed Fringing Reef Lagoon: Ofu, American Samoa

Samantha Maticka, Justin Rogers, Clifton Woodson, Benjamin Hefner, Stephen Monismith

JGR Oceans

RESEARCH ARTICLE
10.1029/2022JC018831

Reef Flat Flow Dynamics for a Nearly Closed Fringing Reef Lagoon: Ofu, American Samoa

Samantha A. Maticka[1,2], Justin S. Rogers[1], Clifton B. Woodson[3], Benjamin B. Hefner[3], and Stephen G. Monismith[1]

[1]The Bob and Norma Street Environmental Fluid Mechanics Laboratory, Department of Civil and Environmental Engineering, Stanford University, Stanford, CA, USA, [2]CNRS, Geosciences Montpellier, Université Montpellier, University of Antilles, Montpellier, France, [3]College of Engineering, University of Georgia, Athens, GA, USA

Key Points:

- Wave driven flows and flow dynamics vary with tidal water level
- Coral reef lagoon appears closed at high tide and open at low tide
- Offshore flows at some depths can develop at times when the lagoon is closed

Supporting Information:

Supporting Information may be found in the online version of this article.

Correspondence to:

S. G. Monismith,
monismith@stanford.edu

Citation:

Maticka, S. A., Rogers, J. S., Woodson, C. B., Hefner, B. B., & Monismith, S. G. (2022). Reef flat flow dynamics for a nearly closed fringing reef lagoon: Ofu, American Samoa. *Journal of Geophysical Research: Oceans*, *127*, e2022JC018831. https://doi.org/10.1029/2022JC018831

Received 7 MAY 2022
Accepted 10 OCT 2022

Author Contributions:

Conceptualization: Samantha A. Maticka, Justin S. Rogers, Clifton B. Woodson, Stephen G. Monismith
Formal analysis: Samantha A. Maticka, Justin S. Rogers, Clifton B. Woodson, Benjamin B. Hefner, Stephen G. Monismith
Funding acquisition: Samantha A. Maticka, Clifton B. Woodson, Stephen G. Monismith
Investigation: Samantha A. Maticka, Justin S. Rogers, Clifton B. Woodson, Benjamin B. Hefner, Stephen G. Monismith
Methodology: Samantha A. Maticka, Justin S. Rogers, Clifton B. Woodson, Benjamin B. Hefner, Stephen G. Monismith
Project Administration: Samantha A. Maticka, Clifton B. Woodson, Stephen G. Monismith
Software: Clifton B. Woodson, Stephen G. Monismith

Abstract We discuss observations of tidally varying wave-forced flows in the reef system on Ofu, American Samoa, a barrier reef and lagoon system that appears open at low tide and closed at high tide. At high tide, the free-surface pressure gradient nearly balances the radiation stress gradient in the depth-integrated momentum equation. At depth, there is an imbalance between these two forces, generating an undertow and flows that turn alongshore, and for some of the time, offshore, behavior similar to rip currents observed on beaches. At low tides, the wave forcing drives purely onshore flows. In general, wave transport is important to determining the total net transport. While the dynamically closed nature of the lagoon mostly suppresses cross-reef transport, there is always some flow through the lagoon with the strongest flows occurring at high tides and when the wave forcing is strongest.

Plain Language Summary Waves and flows observed in the coral reef lagoon system located on the south shore of Ofu, American Samoa, show that flows in the lagoon are driven by incident swell modulated by tidal variations in depth on the steep fore reef and on the shallow reef flat. At low tide, flows are across the reef flat from the fore reef to the lagoon behave as though the lagoon is open to the ocean, whereas at high tide, flows into the lagoon are strongly limited by the resistance felt by the flow out of the lagoon. As a consequence, flows on the reef flat can develop an undertow, as is seen on beaches, although this varies with position on the reef flat. Nonetheless, overall flows in the lagoon are strongest at high tides and weakest at low tides.

1. Introduction

The wave-driven flow through fringing reef-lagoon systems is often described using a one dimensional model (Coronado et al., 2007; Hearn, 1999; Hench et al., 2008; Lowe et al., 2009; Monismith et al., 2013; Sous et al., 2020; Symonds et al., 1995; Taebi et al., 2011; Zhang et al., 2012) and has been shown to be an important flushing mechanism for many reefs (Callaghan et al., 2006; Davis et al., 2011; Hearn, 1999; Hench et al., 2008; Lowe et al., 2009; Munk & Sargent, 1954; Rogers et al., 2017; Symonds et al., 1995), that is, one that is important to determining the response to surface heating (Zhang et al., 2013) or the extent to which benthic communities can change bio-geochemical properties of lagoon waters (Koweek et al., 2015). In the 1D model, waves approach from offshore, shoal, steepen, and break near the reef crest, leading to a setup on the reef flat that drives flow into the lagoon and out through channels in the reef. The area on the fore reef where wave break is referred to as the surf zone; the momentum balance there is between the pressure gradient force (PGF) due to variations in the free-surface height and the radiation stress gradient (RSG). On the reef flat, the balance is generally assumed to be between the PGF and the bottom drag on the reef flat.

The strength of the wave-driven flow over the reef flat depends on the slope of the free surface and thus on the setup of the water level in the lagoon (Lowe et al., 2009). In what follows, a closed lagoon versus open lagoon refers to how easily the incoming ocean water can leave a reef system, a behavior that is determined by the geometry of channel openings (Gourlay, 1996). Using 2D simulations with different idealized geometries, Lowe et al. (2010) found that the lagoon setup varied with the width of the outflow channel: The setup in the lagoon was larger for systems with narrow outflow channels, that is, systems that were nearly closed. In this case, the flow was not one dimensional, but instead was similar to what is seen on beaches, that is, rip currents as a mechanism for water returning to the ocean as opposed to flows out channels (Lowe et al., 2010). These simulations also show that the cross-reef transport is reduced and can be redirected along the reef. Thus, it appears that the 1D

Supervision: Samantha A. Maticka, Clifton B. Woodson, Stephen G. Monismith
Writing – original draft: Samantha A. Maticka, Justin S. Rogers, Stephen G. Monismith
Writing – review & editing: Samantha A. Maticka, Justin S. Rogers, Clifton B. Woodson, Stephen G. Monismith

model best fits systems that have relatively large outlet channels, that is, that appear to be *open*. These two limits might be exemplified by Kāne'ohe Bay as a closed system (e.g., Lowe et al., 2009) and the reef on the north shore of Moorea as an open system (e.g., Monismith et al., 2013).

Using theory and numerical models, Lindhart et al. (2021) investigated how the flow dynamics of an idealized version of the reef-lagoon system found on Ofu, American Samoa, varied tidally. They found that, depending on the water level, the system could be considered either open or closed. They suggested that the extent to which reef systems should be classified as open or closed depends on the momentum balance operating on the reef flat as opposed to the geometry of the reef lagoon. They define open systems as ones exhibiting a balance on the reef flat between an onshore, wave-generated pressure gradient balanced by friction, and closed systems as ones for which the onshore RSG is opposed by an offshore pressure gradient.

In the present paper, we use field observations made on Ofu, American Samoa, in March 2017 to look in detail at the dynamics of flows on the reef flat for times when the Ofu reef-lagoon system appears open and times when it is closed. We examine below the behavior of waves on the reef flat (Section 3.2), the relationship between the setup and wave forcing (Section 3.3), transports on the reef flat and in the lagoon (Section 3.4), and the depth and wave-averaged momentum balance (Section 4). Rogers et al. (2018) describe the general conditions (tides, waves, etc.) observed during this experiment but focus on the connection between the statistics of reef topography and frictional drag in the lagoon. In the present paper, we focus on the behavior and dynamics of the waves and of the wave-driven flows on the reef flat, especially considering the extent to which the system is open or closed.

2. Methods

2.1. Field Site and Instrumentation

All of the measurements we report here were made in and near the reef lagoons on the south shore of Ofu, American Samoa (14.28S, 169.78W) (Figure 1) from March 10 to 28, 2017. Ofu is almost entirely surrounded by a fringing reef extending ca. 100–200 m from the shore. The reef flat itself is about 100 m wide, which is significantly narrower than many other reef sites (Hench et al., 2008; Lowe et al., 2009; Wiens et al., 1962). The reef flat has a tidally averaged depth of ∼0.5 m and has a fairly uniform coverage of roughness features on the order of 5–20 cm high, few of which are living coral. The associated lagoon is ∼2 m deep and has significant coral coverage with features that range from 5 cm to 2 m (Chirayath & Earle, 2016; Oliver & Palumbi, 2009). Physically, Ofu is a common fringing reef-lagoon system, that is, the lagoon axis is parallel to shore and has channels through the reef to connect the lagoon to the ocean. However, compared to systems studied previously (e.g., Hearn, 1999; Hench et al., 2008; Lowe et al., 2009; Coronado et al., 2007), the Ofu reef system has only a few narrow channels as well as higher friction in the lagoon due to the large coral structures. Past work on the south shore of Ofu (Oliver & Palumbi, 2009) has shown that the reef lagoon there can be considered to consist of a set of independent systems, referred to as "pools," with each pool exchanging water more freely with the offshore ocean through the various reef passes than with adjacent pools. Our study focused on flows in pool 400.

The field study employed instruments measuring velocities, pressures, and temperatures throughout the lagoon to observe spatial and temporal variability in both waves and mean flows on the fore reef, in the lagoon and in the exit channel (pass). Figure 1 and Table 1 (see also Maticka (2019)) list the various instruments deployed throughout our 18-day experiment that will be discussed below. In addition to the instruments shown in Figure 1 and that are listed in Table 1, a weather station with sensors for wind speed, wind direction, air temperature, humidity, and incident solar radiation was installed approximately 1,700 m to the southwest near the end of the Ofu airport runway.

In this paper, we focus primarily on the behavior of waves and flows using data from instruments located along the cross-reef D-transect, sites starting with "D," D-3, D-4, D-5, all situated on the reef flat, D0 in the lagoon, and FR5 and FR15 on the fore reef. In what follows, the coordinate system is defined so that x points across the reef and onshore (316°) and y points along the reef and to the southwest (226°). Along this transect, the reef flat is $\sim 135m$ wide and nearly flat with a slight increase in depth toward the lagoon ($dh/dx \approx 4 \times 10^{-3}$ m/m). This line included RBR solo pressure loggers (accuracy = 1 cm; precision = 0.2 mm) except at FR15, where there was a Seabird SBE26+ wave/tide recorder (accuracy = 1 mm; precision < 0.4 mm). At stations D0 and FR15, velocity and wave measurements were made with 2 and 1 Mhz Nortek Acoustic Doppler Profilers (ADPs), respectively. Additionally, 2 MHz Nortek ADPs made similar flow and wave measurements at stations B0, F0, and H0 in

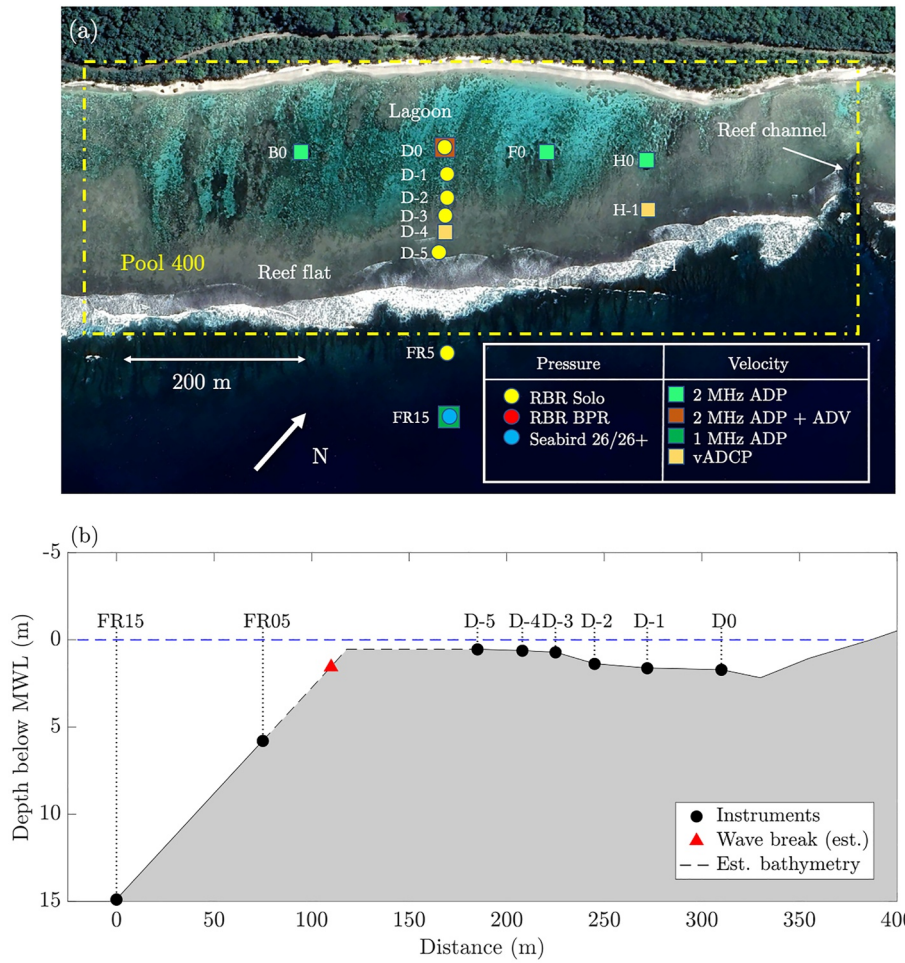

Figure 1. (a) Ofu, American Samoa Pool 400. Locations of instruments deployed in March 2017 deployment. Station D0 is located at (14.17803°S, 169.65325°W); (b) bathymetry (at mean water level) along the cross-shore transect; depths between FR05 and D-5 are approximate. The edge of the white water due to breaking seen in panel (a) is also marked.

the Lagoon. Detailed velocity profiles on 3 s intervals were obtained at D-4 using a Teledyne RD Instruments vADCP configured to run autonomously (Hefner et al., 2019). Unfortunately besides the failure of the vADCP after 5 days due to instrument flooding, the RBR pressure sensor deployed at D-4 also failed to record any data. Nonetheless, because of the unique data provided by the vADCP, the analysis below will primarily focus on those 5 days.

Finally, in addition to moored instruments, several releases of shallow GPS drifters constructed with radio-tracked dog collars (Herdman et al., 2015) were conducted in the lagoon for both high- and low-tide conditions to observe Lagrangian flows in the lagoon.

2.2. Data Analysis

Data from the various pressure and current sensors were analyzed to produce the variation in time of various wave statistics, such as significant wave height and energy flux as follows: All pressure data were divided into half-hour segments and were processed spectrally to (a) correct for frequency-dependent attenuation and (b) compute radiation stresses and energy fluxes (see, e.g., Dean and Dalrymple, 1991). Statistics computed this way match the half-hourly wave burst data acquired by the SBE26+ at station FR15 to the continuous data acquired by the RBR sensors. Wave statistics computed from integration of spectra (e.g., the significant wave height H_s) were further partitioned into swell bands ($0.05\ \text{Hz} < f < 0.33\ \text{Hz}$) and infragravity bands ($0.004\ \text{Hz} < f < 0.03\ \text{Hz}$). Mean water levels were also computed on half-hour intervals for all pressure sensors.

Table 1
Wave and Flow Measurements Ofu March 2017

Station	Location	Depth (m)	Instruments	Sampling
B0, F0, H0	Lagoon	2.28, 1.64, 1.55	2 MHz Nortek ADP	Profile: 3' intervals; 0.15 m bins Waves: Burst 30'; 1,024 samples at 2 Hz
D0	Lagoon	1.72	RBR solo pressure	2 Hz continuous
			2 MHz Nortek ADP	Profile: 3' intervals; 0.15 m bins Waves: Burst 30'; 1,024 samples at 2 Hz
D-1, D-2, D-3, D-5	Reef flat	1.6, 1.4, 0.72, 0.55	RBR solo pressure	2 Hz continuous
D-4	Reef flat	0.65	TRDI vADCP	0.33 Hz; 0.03 m bins; 1st bin: 0.11 mab
FR5	Forereef	5.8	RBR solo pressure	2 Hz continuous
FR15	Forereef	15.4	Seabird SBE26+ Pressure	Tides: 10' (1' avg.); Waves: Burst 30': 1,024 samples at 2 Hz
			1 MHz Nortek ADP	Profiles: 5' intervals; 0.5 m bins Waves: Burst 30': 1,024 samples at 1 Hz
H-1	Reef flat	0.59	TRDI vADCP	0.33 Hz; 0.03 m bins 1st bin: 0.11 mab

Note. Instruments shown are ones referred to in this paper. Further details can be found in Maticka (2019).

The vADCP and ADP data were processed in several different ways: (a) Low-pass filtering using a fourth order Butterworth filter with a cutoff frequency of 0.5 cph to remove all waves and 0.042 Hz to separate infragravity and swell band waves. This pair of cutoff frequencies was used with the vADCP data to examine transport variability associated with wave-averaged flows, infragravity waves, and swell. The low-pass swell-band filter, $\mathcal{F}$, was used to perform wave-averaging, which we will denote in all of what follows for any variable, ψ by $\overline{\psi} = \mathcal{F}(\psi)$. (b) One hour averages of data acquired by the vADCP at station D-4. This was done to balance removal of variability associated with both waves and instrument noise with a temporal resolution of the flow. This approach also facilitated separating wave and mean properties, which could not be done using time series filtering except below the lowest depth (including both tides and waves) recorded at any time by the vADCP.

The volumetric flux per unit width (transport), $q(t)$ was calculated for all profilers (vADCP and ADPs) by integrating the measured velocity profiles ($U_x(z, t)$, $U_y(z, t)$) over depth using the assumption that the velocity was zero at the bed ($z = 0$). In general, this could be done with instantaneous velocities and depths and the result then averaged in time. Doing so would produce the wave-averaged flow:

$$\left(\overline{q}_x, \overline{q}_y\right) = \overline{\int_0^{h+\eta(t)} \left(U_x, U_y\right) dz} \tag{1}$$

Note that if the averaging was applied to the instantaneous transport, the computed wave-averaged flows (shown here for the x direction) include both the mean Eulerian transport, $\overline{q}_{x,E}$ and the wave transport, $\overline{q}_{x,W}$, that is,

the time-averaged transport due to waves (Monismith et al., 2013). This decomposition conventionally involves writing

$$\overline{q}_{x,E} = \int_0^{\overline{h}} \overline{U}_x dz \tag{2}$$

and

$$\overline{q}_{x,W} = \overline{q}_x - \overline{q}_{x,E} \tag{3}$$

For the ADPs in the lagoon, the wave transport was always cross-shore, whereas the mean Eulerian flows were alongshore, and so there was little difference between mean Eulerian flows and overall wave-averaged flows.

However, as we will show below, on the reef flat, wave transport was significant and thus the difference between $\overline{q}_x$ and $\overline{q}_{x,E}$ is important there. To remove wave effects, the transport at D-4 was computed by first averaging the velocity over 1 hr periods, then fitting a cubic smoothing spline to the averaged profile, and lastly setting the upper limit of integration to be a height that was on average below the wave troughs, that is, $z = \overline{h} - H_s/2$, where H_s is the significant wave height. Unfortunately, there were two problems with directly computing the wave transport using the vADCP data: (a) the relatively low-sampling frequency of the vADCP (0.3 Hz) and (b) the fact that depth for the vADCP was measured using surface tracking. Both of these problems meant that the swell-band waves were not fully resolved, potentially causing the wave transport computed per Equation 3 to be smaller than the actual value.

One way to assess the ability of the vADCP to accurately measure the wave-induced velocity is to look at the velocity data in light of shallow water theory, which gives the instantaneous wave-induced velocity (which is independent of depth), $\tilde{U}_x$ as a function of the instantaneous free-surface deflection $\tilde{\eta}$ and mean depth, h:

$$\tilde{U}_x = \frac{\tilde{\eta}\sqrt{g\overline{h}}}{h} \tag{4}$$

In terms of the wave-averaged transport, Equation 4 implies that

$$\overline{q}_{x,W} = \frac{\eta_{rms}^2\sqrt{gh}}{h} \tag{5}$$

whereas casting Equation 4 in terms of rms values of U_x and η provides a good description of the vADCP velocities, the measured instantaneous velocities are poorly correlated with ($r^2 = 0.09$) and are only ca. 30% as large as theoretical values. As a consequence, the computed wave transports are significantly less than what would be calculated using 5.

The closest instrument to the vADCP that could have properly resolved wave motions and thus can be used to test Equation 5 was the ADP at D0. In this case, the observed wave transports were 40% of what would be predicted by Equation 5 ($r^2 = 0.78$). As seen in the vADCP data, velocities more closely matched theory, with Equation 4, albeit with a constant of 0.84 rather than 1 ($r^2 = 0.82$). Moreover, η_{rms} at D-4 inferred from surface tracking matches well values of η_{rms} that would be estimated by interpolation of values of η_{rms} between D-5 and D-3. Thus, while the vADCP surface tracking may have resolved most of the surface wave variance, it did not properly resolve the wave transport, possibly an effect of noise. Thus, in the absence of any better estimate, we computed the wave transport at D-4 using measured values of η_{rms} and Equation 4 multiplied by 0.4.

Finally, the quantification of the fidelity of the various models used to describe aspects of the hydrodynamics of the Ofu reef was done using both the coefficient of determination (r^2) and the Willmott skill score (referred to as "skill"—Willmott, 1981).

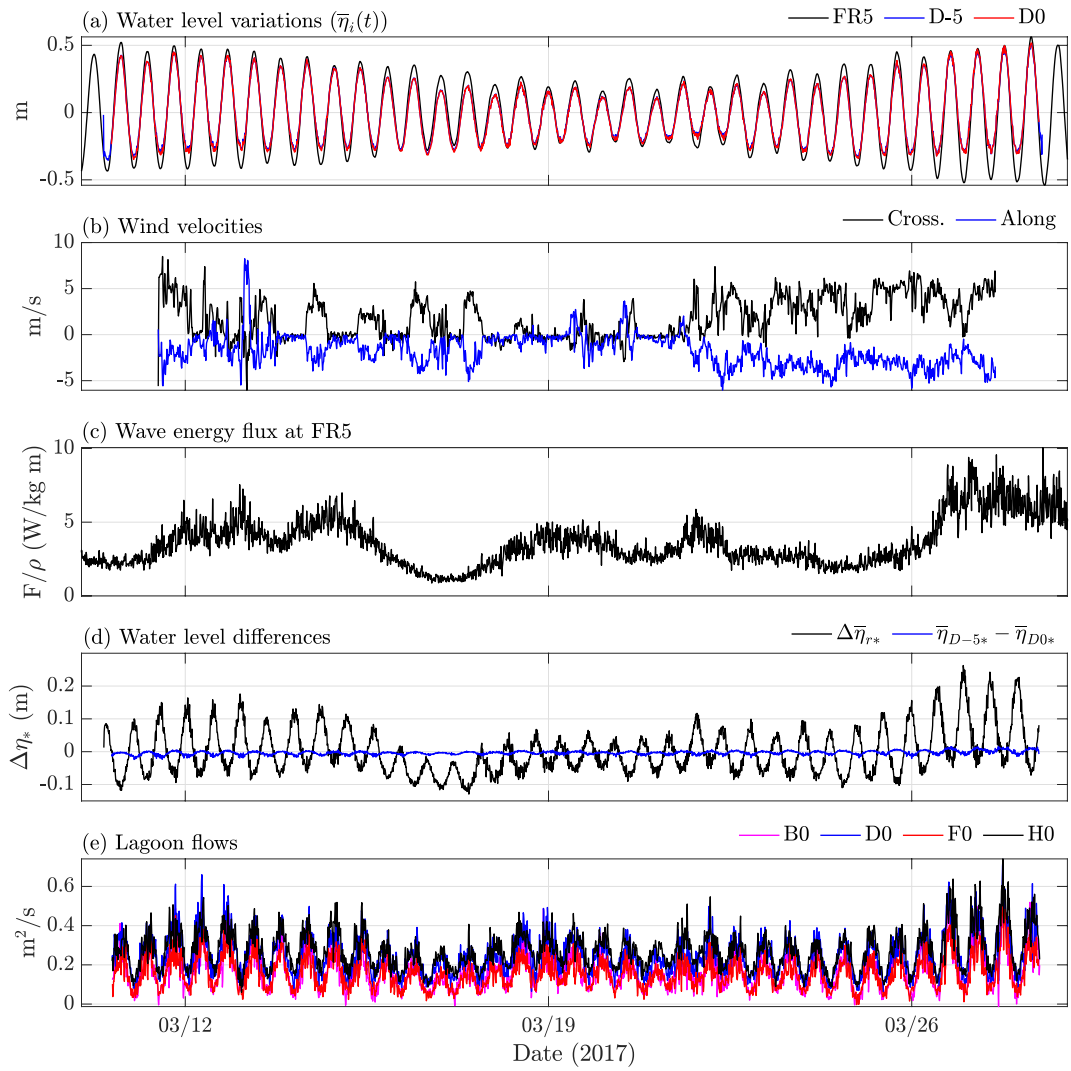

Figure 2. Field conditions during the study. (a) Water level variations; (b) wind velocities; (c) wave energy flux on the fore reef (FR5); (d) water level differences fore reef to reef flat $\left(\Delta\overline{\eta}_{r*} = \overline{\eta}_{D-5*} - \overline{\eta}_{FR5*}\right)$ and reef flat to lagoon $\left(\overline{\eta}_{D0*} - \overline{\eta}_{D-5*}\right)$; (e) lagoon alongshore transports (positive toward the channel).

3. Observations

3.1. Forcing

During this study, the fore reef tidal range was ~1 m (Figure 2a), resulting in water depths on the reef flat ranging from ~35 cm to 1 m at D-5. The wind was weak, with speeds less than 5 m/s, and typically toward the west (positive cross- and negative alongshore components) (Figure 2b). The wind-induced surface stress, τ_s, was estimated using a quadratic drag law, $\tau_s = C_D \rho_{air} U_a |U_a|$, where $\rho_{\text{air}} = 1.23$ kg/m^3 is the density of air, $C_D = 0.0008$ is the drag coefficient for wind velocities less than 6.6 m/s (Hellerman, 1967), and U_a is the wind velocity. Thus, on average, $\tau_s \simeq 0.005$ Pa and had a maximum value of ca. 0.033 Pa. Thus, wind stresses were much smaller than the other measured forces on the reef flat (see below) and so will be neglected in the rest of what follows.

Figures 2c and 2d shows: (a) the connection between wave forcing, calculated spectrally as in Monismith et al. (2015) using the pressure data at FR5 corrected for frequency-dependent attenuation, and the setup between the fore-reef (FR15) and the ocean-ward edge of the reef flat (D-5); and (b) the very small sea surface elevation difference across the reef flat (i.e., between D0 and D-5). The setups shown are calculated as the wave-averaged depths minus the average depth for the whole record, that is, for any location

$$\bar{\eta}_* = h - \frac{1}{T_R}\int_0^{T_R} h dt \tag{6}$$

where h is the measured wave-averaged depth, and T_R is the length of the record. Unfortunately, this approach also removes the mean setup, which must be found separately, a procedure we describe below (see also Monismith et al. (2013)). Here, the * subscript is used to indicate that Equation 6 does not result in the deviation in free-surface position from the level that would exist in the absence of tides and waves. As seen in Figure 2, cross shore variations in the water level on the reef flat were approximately 10 times smaller than were those between the fore-reef and the reef flat; thus, as described by Lindhart et al. (2021), the Ofu lagoon appears to be "closed." The dynamics of the reef flat flows will be explored further below. Nonetheless, flows in the lagoon are in phase with tidal elevation and are clearly related to the strength of the wave forcing (Koweek et al., 2015). Thus, the Ofu reef might be better described as "mostly closed"in that waves do force flows through the lagoon despite the high resistance associated with large roughness in the lagoon (see Rogers et al. (2018)) and the narrow exit channel between pools 400 and 500. Wave forcing on the fore reef consisted of longer-period (12–22 s) swell events and local short-period (4–7 s) waves, with H_{rms} ranging from ∼0.4–1 m (Figure 3), that broke normal to the crest ($-0.8° \pm 2.3°$). Applying the approach of Sheremet et al. (2002) (their Equations 2 and 3) to the FR15 ADP wave burst velocity and pressure data, we found that ca. 10% of the sea-swell (SS) wave energy flux was reflected seaward off the fore reef (Maticka, 2019). Due to this relatively small amount of reflection and the near-normal wave direction on the reef, we assume in our analysis below that 100% of the energy flux is shoreward.

3.2. Waves on the Reef Flat

Offshore of the reef crest, virtually all of the wave energy was in the sea-swell band, whereas inshore of breaking, the wave energy in the infra-gravity wave and swell bands was similar (Maticka, 2019) (see Figure S1 in Supporting Information S1). As is commonly found (e.g., Lowe et al., 2009), waves on the reef flat varied with the water level (Figure 3) with ∼60% reduction in H_{rms} from high tide to low tide. Evidently, for the Ofu reef, the majority of tidal variations in the wave height takes place on the shallow fore reef where breaking occurs (Maticka, 2019). Unlike what is seen on beaches (e.g., Raubenheimer et al., 1996), inshore of D-5, local wave height was not a constant fraction of the local depth (Figures 3k–3m), suggesting that bottom friction (BF) may be more important than depth-limited wave breaking for dissipating energy on the reef flat.

The relative importance of breaking and BF can be assessed by modeling the observed reduction of swell-band wave energy flux, F, between D-5 and D-3 caused both by dissipation due to wave breaking and BF:

$$\Delta F = -(\varepsilon_B + \varepsilon_F)\,\Delta x \tag{7}$$

where ε_B is the dissipation due to breaking modeled, here calculated using the formulation of Thornton and Guza (1983) (hereafter TG83), and $\varepsilon_F = 0.6 f_w U_{\text{rms}}^3$ is the dissipation due to BF with friction factor f_w and rms wave velocity U_{rms}. This combined model has three parameters, two from TG83, γ, and B, an O(1) scaling constant, and f_w. As suggested by Roelvink (1993), γ and B may not be independent, although, following Thornton and Guza (1983), we assumed that they are independent. Three possible combinations of these two processes are shown in Figure 4 where, in each case, the parameters have been chosen to provide a least squares fit equating measured and modeled dissipation rates. In both cases with breaking, we have assumed that $\gamma = 0.87$, the value we derive below from the mean setup; in the mixed case, we assume $B = 1.7$ as found by TG83, whereas in the first case, we choose the somewhat high value of $B = 3.29$ to best match the observed dissipation. Similar fits gave $f_w = 0.22$ without breaking and $f_w = 0.19$ with breaking, values comparable to what has been observed on some reefs (e.g., Lowe et al., 2009) but only about 20% of the value found by Lentz et al. (2016) for a reef flat in the Red Sea. Perhaps not surprisingly, it is clear that models with BF (Figures 4b and 4c) perform significantly better than does the model with breaking alone (Figure 4a); that is, both r^2 and the skill score are higher for the BF models than that for the breaking model. For the case with both breaking and BF, breaking provided about 10% of the total change in energy flux between D-5 and D-3.

Nonetheless, waves on the reef flat did resemble those seen in beach surf zones. Their visual appearance was bore-like, that is, they were highly turbulent and aerated near the steep, front face where breaking appeared to be taking place (Figure 5). A transformation of the incoming bores into trains of nonlinear solitary-like waves, that

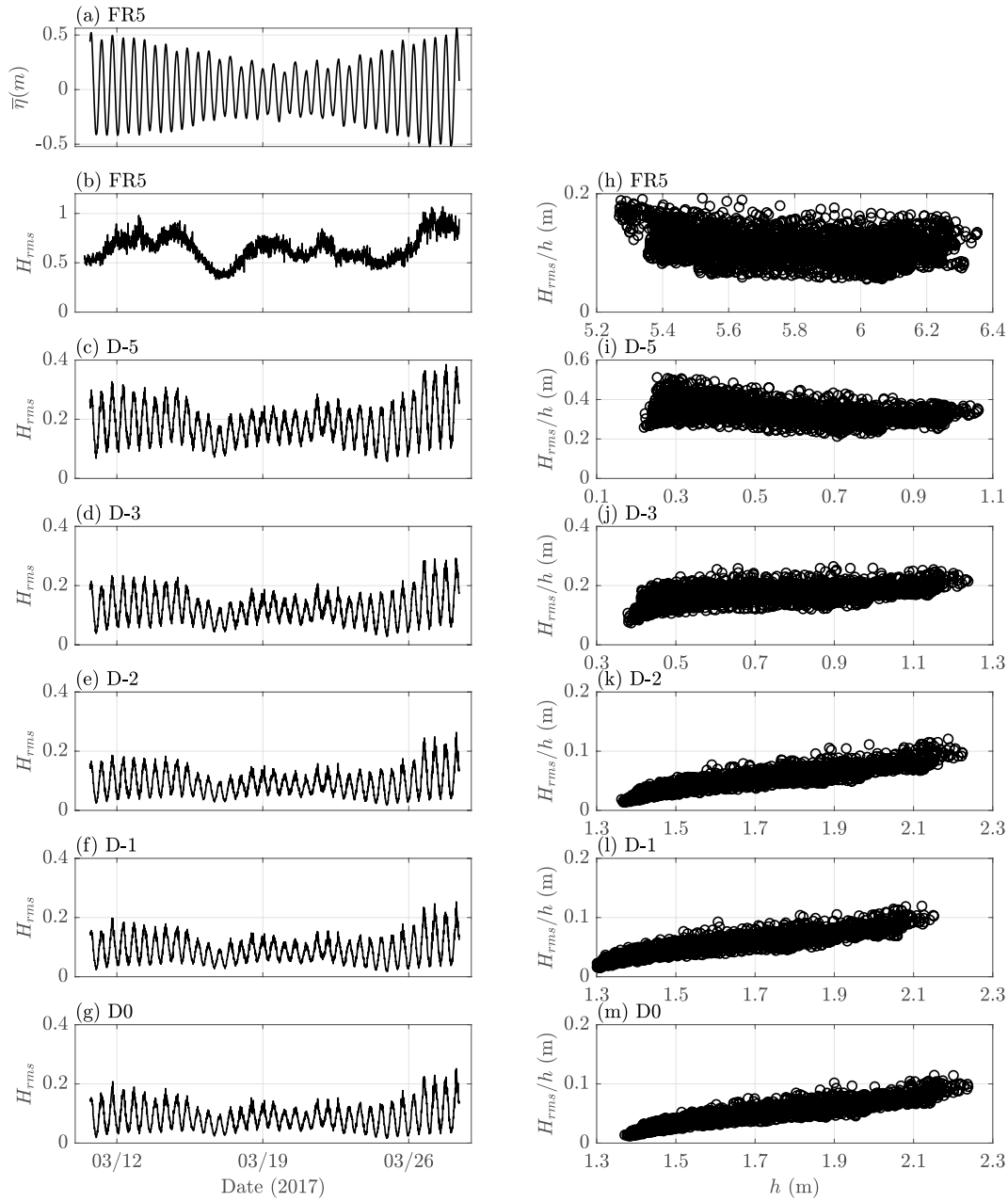

Figure 3. (a) Depth at FR5. (b–g) root mean square (RMS) wave heights on the D transect line. (h–m) RMS wave height for normalized by depth as a function of depth for the same stations shown in (a–e).

is, into a set of rank ordered waves in each wave train can also be seen in Figure 5, most notably at high water. The Ofu reef flat waves are notably asymmetrical: calculated asymmetries (Elgar & Guza, 1985) for stations D-5 and D-3 were comparable (−0.7 to −2) to those calculated for broken waves observed in the surfzone, for example, −0.5 to −1 as reported by Raubenheimer et al. (1995) (see Figure S2 in Supporting Information S1).

3.3. Free-Surface Response to Waves

The setup or setdown of the free surface relative to offshore, $\overline{\eta}_r$, represents the wave-averaged effect of wave forcing on the free surface (Longuet-Higgins & Stewart, 1964; Mei et al., 1989). As shown by Vetter et al. (2010), in the absence of frictional dissipation, this setup depends on the incident wave energy flux, F, the depth on the reef flat, h_r, and the breaking depth fraction for depth-limited breaking, γ,*viz*,

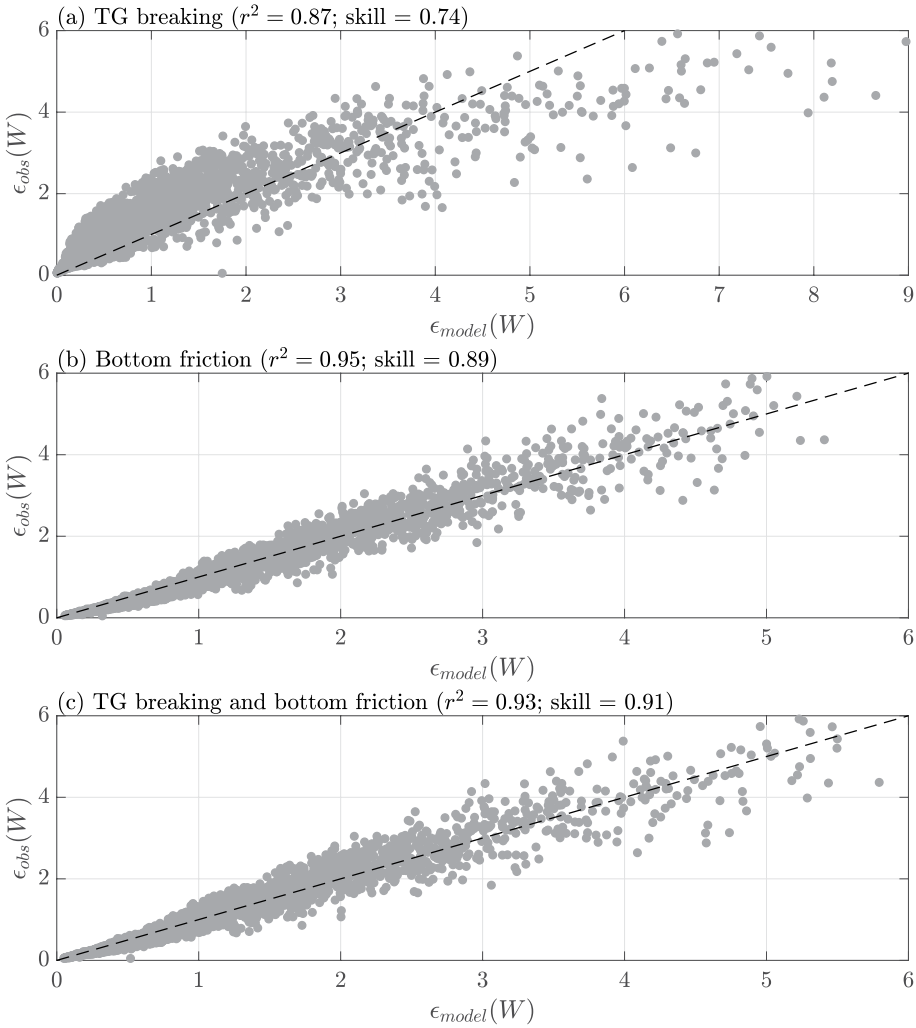

Figure 4. (a) Wave dissipation by breaking only. Modeled using Thornton and Guza (1983) with $\gamma = 0.87$ and $B = 3.29$; $r^2 = 0.68$ and skill = 0.74. (b) Wave dissipation by bottom friction (BF) only with $f_w = 0.22$; $r^2 = 0.95$ and skill = 0.89. (c) Wave dissipation by wave breaking ($\gamma = 0.87$ and $B = 1.7$) and BF ($f_w = 0.19$); $r^2 = 0.93$ and skill = 0.91. In all cases, what is shown is the average dissipation between D-5 and D-3.

$$\overline{\eta}_r \simeq \frac{3\gamma^2}{8+3\gamma^2}\left(\frac{(8F/\rho)^{2/5}}{g^{3/5}\gamma^{4/5}} - h_r\right) \tag{8}$$

thus, per Equation 8, the amount of setup may vary with the tides due to tidally modulated breaking (Callaghan et al., 2006): As the water level decreases, the setup on the reef increases. Per Equation 8, there will be a limiting value of F for a given value of h_r for which there is no breaking and hence no setup. Generally, γ depends on the geometry of the reef (beach), that is, fore-reef (beach) steepness (Becker et al., 2014; Raubenheimer et al., 1996) and the presence or absence of a reef crest ridge (Yao et al., 2012); thus, at present, γ should be viewed as a free parameter to be determined from observations.

In the present case, we defined $\overline{\eta}_r$ as the difference in the wave-averaged sea level height between the fore reef and the first reef flat station, that is, $\overline{\eta}_{D-5} - \overline{\eta}_{FR15}$. Note that this assumes that the water level is flat between wherever breaking ceases being depth-limited and D-5. Computing setups using Equation 6 removes any mean differences in elevation between the pressure sensors, but also removes the mean setup. Thus, there is an offset that must be determined using additional information. Based on Equation 8, the depth of no setup can be estimated by plotting $\Delta\overline{\eta}_{r*} = \overline{\eta}_{D-5*} - \overline{\eta}_{FR5*}$ as a function of F and fore reef depth. Doing so, we find that the offset between FR5 and D-5 is $\simeq$ 12 cm (see Supplementary material Figure S3 in Supporting Information S1), that is, $\Delta\overline{\eta}_r = \Delta\overline{\eta}_{r*} + 0.12$.

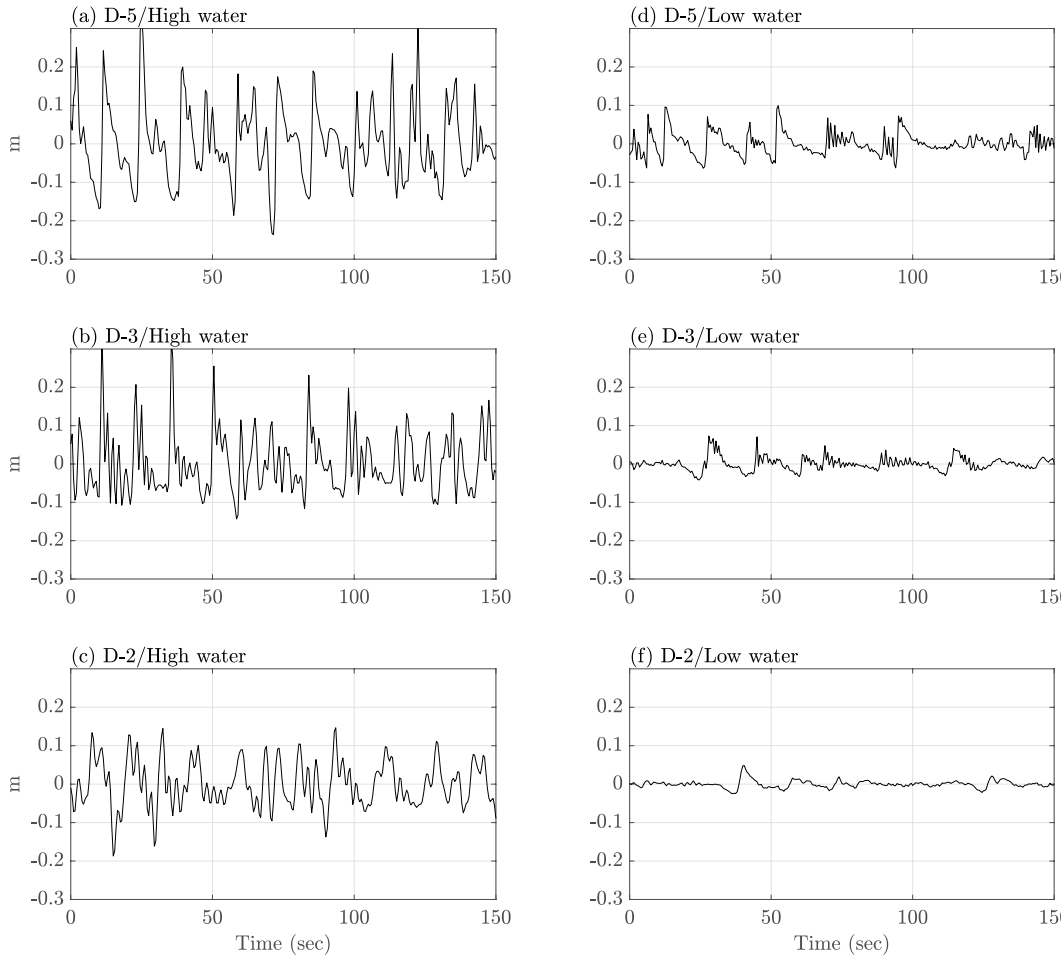

Figure 5. Sample water surface records on the reef flat at D-5, D-3, and D-2. (a–c) High water (12 March 2017 07:23:14). (d–f) low water (12 March 2017 00:59:04).

Predicted and observed setup time series using this value and $\gamma = 0.87$ and h_r varying tidally with a minimum depth of 0.25 m are shown in Figure 6.

The setup calculated on the reef flat (D-5) was generally consistent (skill = 0.85; $r^2 = 0.92$) with predictions made using Equation 8, where $\overline{\eta}_r$ increases with wave energy flux and decreases with reef depth as a result of tidally modulated wave breaking (Figure 6c). The error in model predictions (Figures 6d and 6e) was generally small (rms error = 2 cm); arguably, this reflects changes in breaking dynamics. In principle, γ could be made a function of fore reef depth to better match the observations as was done by Becker et al. (2014), but this would not likely have much generality. Nonetheless, the value of γ found here is similar to that found by Monismith et al. (2013) for the Moorea fore reef (0.98) and by Becker et al. (2014) for the reefs at Roi-Namur and Ipan (0.7–1.3).

The setup in the lagoon (D0) followed the same trend with little difference (<1 cm) in free-surface elevation between the reef flat and the lagoon (Figure 2d). This is the behavior that is expected for a closed lagoon (Gourlay, 1996; Lowe et al., 2010), that is, a nearly spatially uniform setup in the cross-shore direction. In contrast, the free-surface height in an open lagoon will be equal to that of the offshore ocean (Symonds et al., 1995). Evidently, for the case of Ofu, the combination of high friction in the lagoon (Rogers et al., 2018) and the narrowness of the exit channel relative to the overall alongshore length of the lagoon (20 m vs. ca. 500 m) combine to create a relatively closed system.

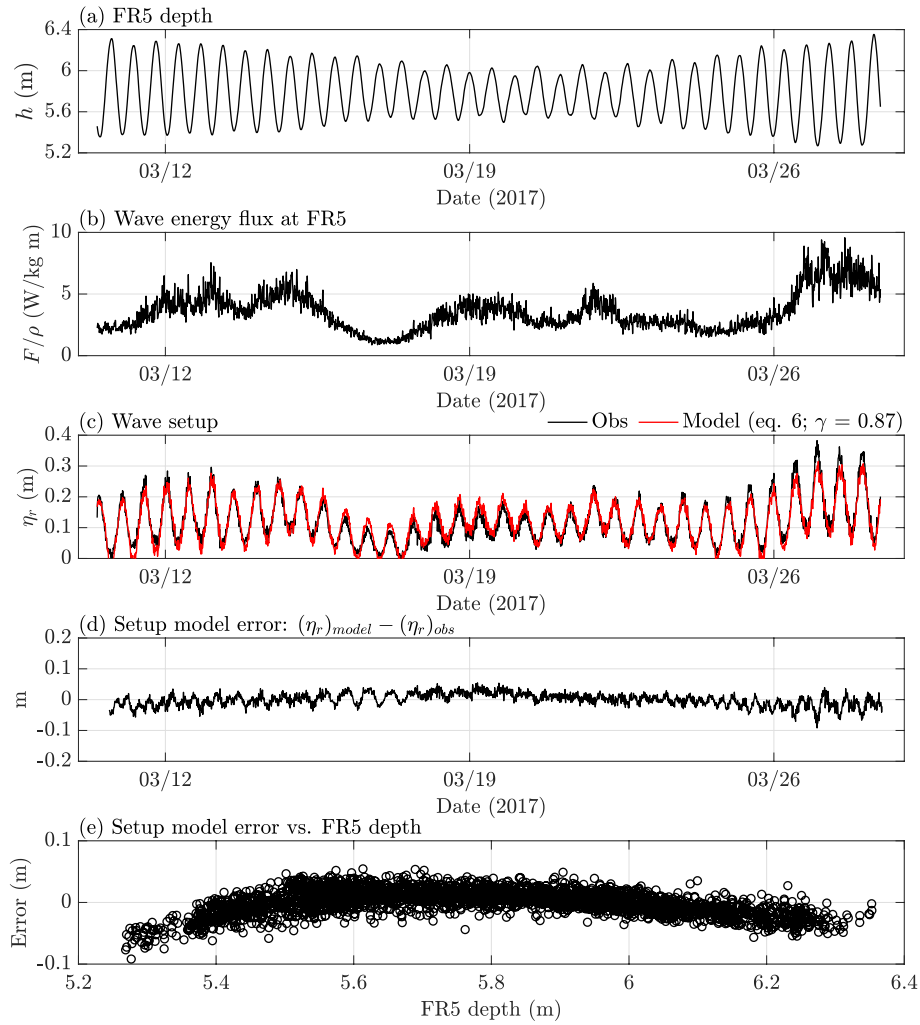

Figure 6. (a) Depth on fore reef (FR5); (b) wave energy flux at FR5; (c) observed and modeled setups on reef flat; (d) error in the predicted setup as a function of time; (e) error in the predicted setup as a function of fore-reef depth.

3.4. Flows on the Reef Flat

While the difference in the setup between the reef flat and the lagoon was small, there was flow across and along the reef flat (Figure 7). The cross-reef flows were strongly sheared, with offshore flows near the bottom at high tide early in the record, and over nearly all of the depth at high tides in the later part of the record. Throughout the record, flows were onshore at low tides. The transition between these two conditions took place near when $\overline{\eta} \simeq 0$. In contrast to the strongly sheared cross-reef flows, the alongshore flows were nearly unsheared and were primarily directed toward the channel to the northeast when the free surface was above the mean water level.

The transport in the lagoon was mostly directed alongshore and had a strong tidal variation, but with a magnitude that was dependent on the strength of the wave forcing on the fore reef (Figure 2e). On the reef flat, the vADCP resolved approximately 90% of instantaneous depth. Thus, because the averaging was applied to the instantaneous transport, the computed wave-averaged flows (shown here for the x direction) include both the mean Eulerian transport, $\overline{q}_{x,E}$, and $\overline{q}_{x,W}$, the time-averaged transport due to waves (Monismith et al., 2013).

Figure 8 shows that the wave-associated transports, that is, the swell and infragravity band flows were roughly an order of magnitude larger than the wave-averaged mean Eulerian flow with swell band and infragravity wave band flows being comparable to each other. While the instantaneous flows were wave-dominated, the estimated

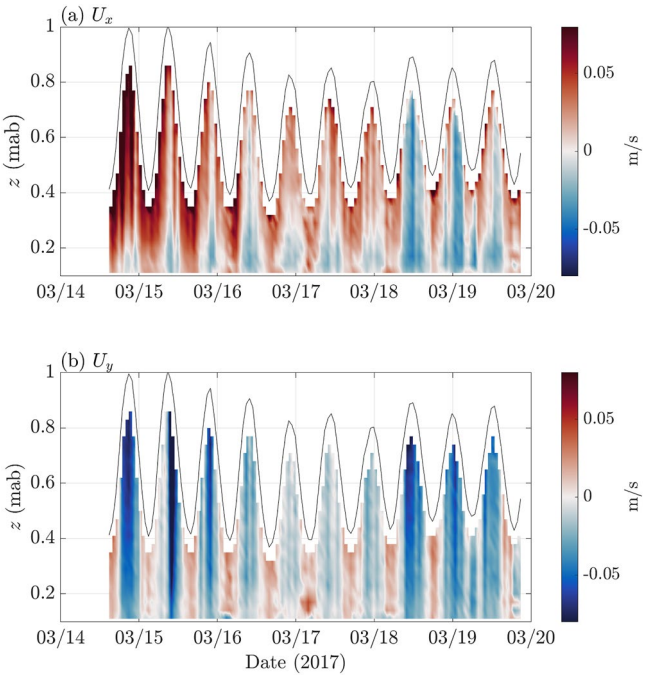

Figure 7. vADCP measured velocities at D-4: (a) Cross-reef flows (positive onshore); (b) along-reef flows (negative directed toward the channel).

wave transport on the reef flat described by Equation 5 (multiplied by 0.4) was comparable to and generally less than the mean Eulerian transport.

Overall, there was a striking reversal of the wave-averaged cross-reef Eulerian flow such that during the latter part of the record shown in Figure 8, flow was nearly directed offshore at times. This behavior is strikingly different from what has been reported for other barrier reefs, the appearance of an "undertow," that is, an offshore-directed Eulerian mean flow is something that is commonly seen on beaches. Another distinctive feature of flows on the Ofu reef flat is that the along reef flow is comparable to the cross-reef flow such that at high tides, flow on the reef flat is directed toward the channel between pools 400 and 500 rather than either onshore or offshore. As a result, the flow direction alternates between primarily cross shore at low tide and primarily alongshore at high tide.

The vertical structure of the flow (Figure 9) shows clearly the change in the flow structure between high tides and low tides. At high tides, the near-bottom flow can be offshore when the overall flow is onshore (e.g., Figures 9a and 9j) and is offshore over much of the depth when the overall flow is also offshore (Figures 9g–9i). In contrast, the flow was always onshore at low tides.

As shown by Svendsen (1984) (see also Henderson et al., 2017; Reniers et al., 2004; Roelvink & Reniers, 2011), the vertical structure of surfzone flows like those we observed on the Ofu reef flat is determined by the local force imbalance that arises because the radiation stress varies with depth with the part (2/3 in shallow water) of the wave contribution to momentum flux occurring between the trough and crest and part (1/3 in shallow water) occurring below the trough (Svendsen, 1984). However, depending on the strength of BF, the pressure gradient that is constant over depth, approximately balances the entire radiation stress. Thus, when the pressure gradient is directed offshore and thus opposes the RSG, it can produce an offshore flow near the bottom, that is, an undertow. As we discuss below, for the Ofu reef, what is important is that the radiation stress covaries with the tidal elevation such that the net force also varies through the tidal cycle, thus leading to tidal variations in undertow.

In addition to the vADCP observation of undertow, Lagrangian drifter tracks (see Maticka, 2019) show that besides the main channel, offshore flows were also consistently present near station H-1, a behavior seen in the vADCP data taken there and discussed in Hefner et al. (2019). However, at high tides, offshore flows also appeared near the D-transect, a behavior that is similar to rip currents that develop on beaches (MacMahan et al., 2006) (see Figure 1 in Rogers et al. (2018)). For the Ofu reef, the fact that outflows take place at consistent locations other than in the main channel may reflect the way small variations in reef crest topography can support relatively stable, but tidally variable, plan-form variable currents. On the other hand, for low tides, flows were toward and out of the channel, conditions seen in other, more "open" systems (Hench et al., 2008; Symonds et al., 1995).

In summary, the flows we observed at high tide differed from what would be expected of the simple 1D model and are consistent with predictions from numerical simulations of closed reef-lagoon systems, for which rip currents and along-reef flows might be expected (Lowe et al., 2010). Additionally, we observed an undertow, something not captured in the simulations of Lowe et al. (2010) since their model did not resolve the vertical flow structure. In contrast, the low tide conditions are consistent with the standard 1D conceptual model of wave-driven flows, that is, there is flow shoreward over the reef flat, then along the lagoon toward the channel, and then out the exit channel.

4. The Depth-Integrated Momentum Balance on the Reef Flat

Due to the narrowness of the Ofu reef flat (ca. 100 m), the incident waves, while broken, were not fully dissipated by the time they reached the reef flat stations (D-5, D-4, and D-3). As the water level decreased with the tide, the fraction of waves that broke on the fore reef increased, which decreased wave height and energy on the reef flat,

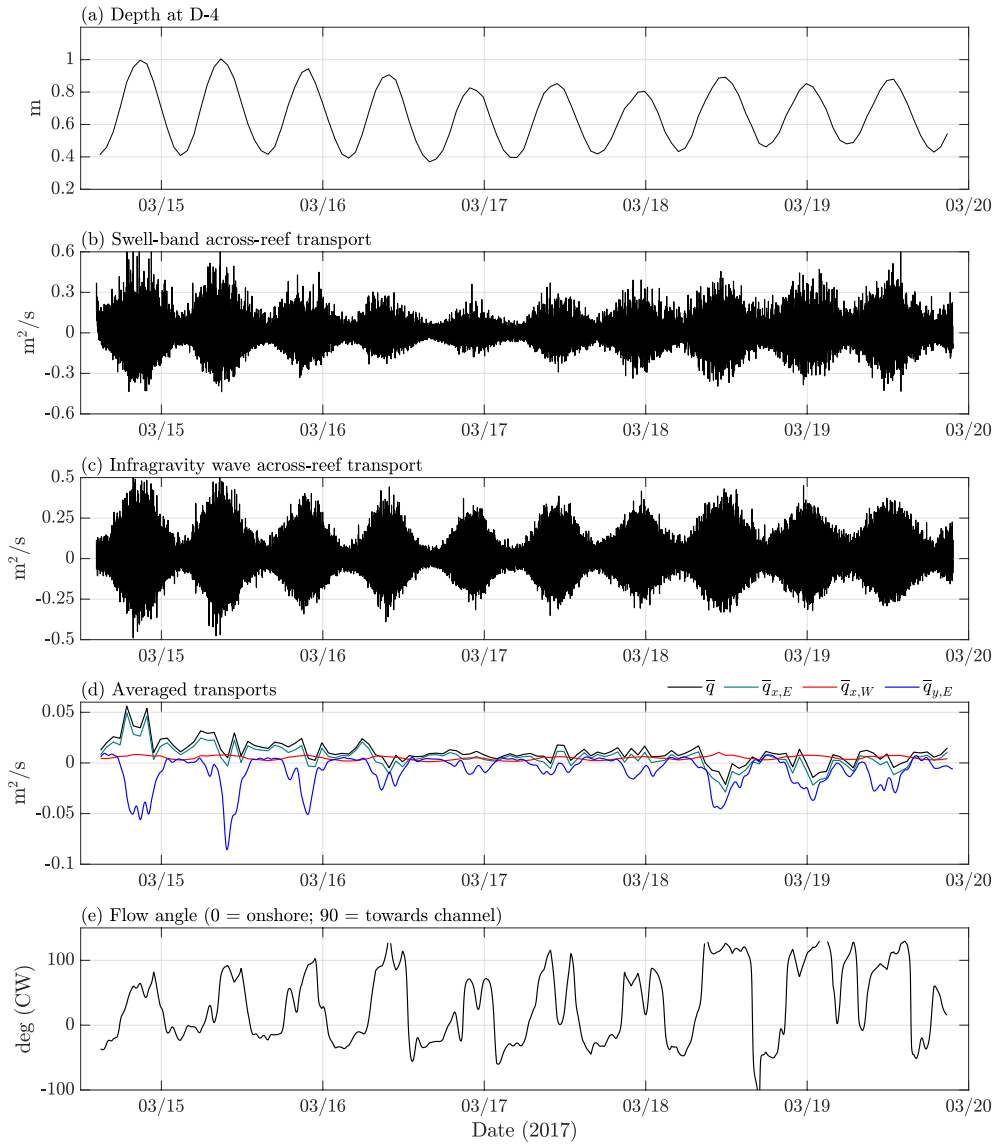

Figure 8. Depths and flows at D-4: (a) Depth; (b) instantaneous swell band wave transport; (c) infragravity wave transport; (d) wave-averaged transports in the cross-shore (x) and along-shore directions (y); (e) angle of the wave-averaged mean Eulerian flow relative to the x direction (positive clockwise (CW)). All transports except q_w were measured by the vADCP.

but increased the amount of setup on the reef flat. In this section, we examine the dynamics of the depth-averaged flow and free-surface variations using the depth-integrated momentum balance of the cross-reef flow, an analysis that will be done for the section of the reef flat between D-5 and D-3, using the vADCP measurements at D-4. We note that more recent 1D models of surf-zone flows on beaches can be found (e.g., in Ruessink et al. (2001), Apotsos et al. (2007), and Henderson et al. (2017)).

The cross-shore component of the 1D steady, wave-averaged, depth-integrated momentum equation commonly used to describe nearshore flows is (Apotsos et al., 2008; Mei et al., 1989; Ruessink et al., 2001):

$$\frac{d}{dx}\left(\frac{\overline{q}_x^2}{h+\overline{\eta}}\right) = -g\left(h+\overline{\eta}\right)\frac{d\overline{\eta}}{dx} - \frac{1}{\rho}\frac{dS_{xx}}{dx} - \frac{1}{\rho}\frac{dR}{dx} - \frac{\tau_b}{\rho} \tag{9}$$

where x is the principal flow direction (i.e., cross-reef), h is water depth, $\overline{\eta}$ is time-averaged free-surface height deviation from mean sea level, τ_b is the bottom stress, S_{xx} is radiation stress due to waves (calculated spectrally),

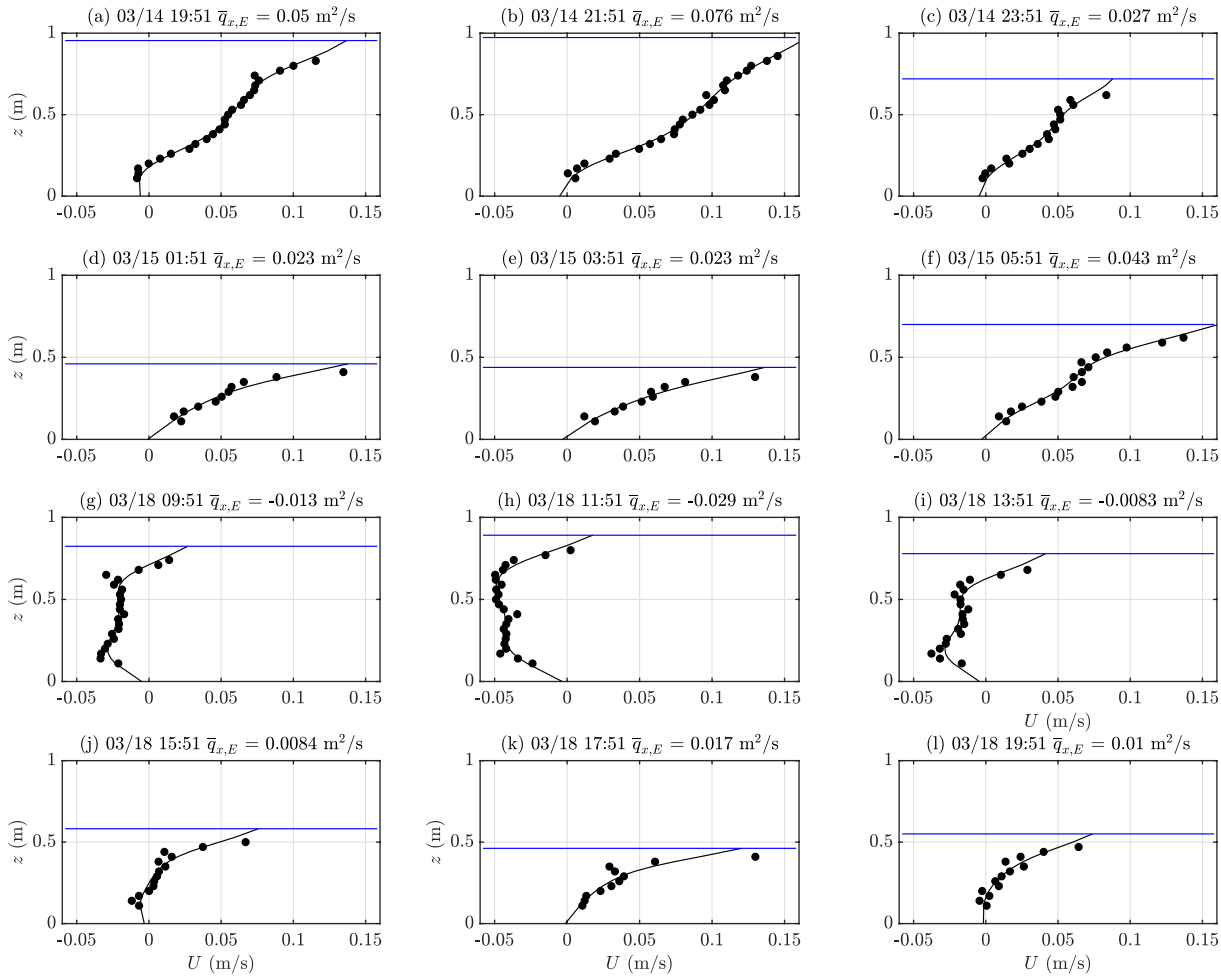

Figure 9. vADCP cross-shore velocity profiles measured at D-4 near high water (a-c and g-i) and near low water (d-f and j to l). The horizontal blue line in each panel shows the mean location of the free surface. The black line shows a cubic spline-smoothed (smoothing parameter = 0.9995) fit to each velocity profile that was used to compute $\overline{q}_{x,E}$. Times and values of $\overline{q}_{x,E}$ for each profile are shown in the figure. For panels (a–f), the mean Eulerian flow was always onshore, whereas for panels (g–l), the mean Eulerian flow was offshore at high tide and onshore at low tide.

and R is the extra contribution to the wave forcing due to the presence of surface rollers (Svendsen, 1984). From left to right, the terms in Equation 9 will be referred to as advection (ADV), PGF, RSG, roller force (RF), and BF. It is important to note that the flow appearing in Equation 9 is the total flow q, that is, the flow including both Eulerian and wave transports (Mei et al., 1989; Monismith et al., 2013).

Advection is often not important in reef-lagoon systems (Sous et al., 2020). For the reef flat at Ofu: $\overline{q} \approx 0.05\, m^2/s$, $h \approx 0.5$ m, $dq/dx \approx 0$ (from 1D continuity), $dh/dx \approx -4 \times 10^{-3}$ m/m (see Maticka (2019)), and $\overline{\eta} \ll h$. Thus, we estimate:

$$\rho \frac{d}{dx}\left(\frac{\overline{q}_x^2}{h}\right) = \rho\left(\frac{2\overline{q}_x}{h}\frac{d\overline{q}_x}{dx} - \frac{\overline{q}_x^2}{h^2}\frac{dh}{dx}\right) = -\rho\frac{\overline{q}_x^2}{h^2}\frac{dh}{dx} \approx 4x10^{-2} Pa \tag{10}$$

For most of our study period, this is 1–2 orders of magnitude smaller than our estimates for the other forces. As with wind stresses, advective accelerations are neglected in what follows.

Thus, neglecting advection, we write Equation 9 as

$$-\frac{1}{\rho}\frac{dS_{xx}}{dx} - \frac{1}{\rho}\frac{dR}{dx} = g\left(h+\overline{\eta}\right)\frac{d\overline{\eta}}{dx} + \frac{\tau_b}{\rho} \tag{11}$$

where the LHS represents the wave forcing, and the RHS represents the possible response. For reef flats in open systems, both the RHS and LHS are zero, that is, the wave forcing is nearly zero and the pressure gradient across the reef balances bottom drag (cf. the Moorea reef—Monismith et al. (2013)), whereas for closed systems, for example, beaches, the wave forcing is balanced by the pressure gradient, and the flow and thus the bottom drag are small. We will consider each of the terms in Equation 11 in turn below.

The RSG ($-dS_{xx}/dx$) is calculated using finite differences as $-dS_{xx}/dx \simeq -\Delta S_{xx}/\Delta x$ where Δx is the cross-shore distance from D-5 to D-3. ΔS_{xx} was calculated by differencing the results of spectral integration of the wave data at D-5 and D-3 including both the sea and swell and the infragravity frequency bands ($f_1 - f_2 = 0.004$–0.25 Hz):

$$S_{xx} = \rho g \int_{f_1}^{f_2} P_{\eta\eta}(f,t) \cdot \left(2\frac{C_g}{C} - \frac{1}{2}\right) df \tag{12}$$

where f is the frequency, t is time, C_g is wave group velocity, C is wave phase speed, and $P_{\eta\eta}$ is the spectral density of variations in the free-surface height modified to account for frequency-dependent attenuation of the pressure.

The RF is more problematic since it depends on knowing, or being able to calculate, the roller area, A_r (Ruessink et al., 2001). While Svendsen (1984) assumed that $A_r = 0.9H_{\text{rms}}^2$, later 1D surf zone models (e.g. Ruessink et al., 2001) solve for the evolution of the roller as well as solving for the waves themselves. In the present case, this is not really possible since the source term for the roller is the rate of breaking dissipation, which is likely uncertain since breaking on the reef face and continued breaking on the reef flat appear to be different from what the standard surf zone models describe. As a simple alternative, we examined using the approach of Svendsen (1984), modified by changing the scaling coefficient from 0.9 to the value of 0.3 derived by Martins et al. (2018), finding that R was less than 3% of S_{xx}. Accordingly, we did not include R in any subsequent calculations.

While the wave forcing can be calculated explicitly, the PGF and BF terms both include parameters that are unknown a priori. The free-surface slope on the reef flat shown in Figure 2 does not include whatever the mean setup might have existed during our field experiment. If a quadratic drag law is used, then the drag coefficient, C_D, must also be determined in some fashion. In what follows, we will pursue an iterative approach to estimate both the unknown mean setup and C_D.

The 1D wave-averaged quadratic drag law

$$\overline{\tau_b} = \rho C_D \overline{U_x \left(U_x^2 + U_y^2\right)^{1/2}} \tag{13}$$

is often used to represent bottom stress (Grant & Madsen, 1979; Lentz et al., 2017), where (U_x, U_y) is the depth-averaged Eulerian velocity, and C_D is the drag coefficient. When waves are present, the velocities appearing in Equation 13 include both wave averaged velocities and the wave velocities, that is, $U_x = \overline{U}_x + \tilde{U}_x$ (Feddersen et al., 2000). Thus, the bottom drag acting in the x direction will be

$$\overline{\tau_b} = \rho C_D \overline{\left(\overline{U}_x + \tilde{U}_x\right) |\overline{V} + \tilde{V}|} \tag{14}$$

where $V = \left(U_x^2 + U_y^2\right)^{1/2}$. If $\tilde{V}_{rms} \gg \overline{U}_x$, then $\overline{\tau_b} \simeq 2\rho C_D \overline{U}_x \tilde{V}_{rms}$ (Wright & Thompson, 1983).

For the surface slope, we started with the difference in $\overline{\eta}_*$ (defined by Equation 6) between D-2 and D-5 (60 m separation) rather than between D-3 and D-5. The reason for using these two stations rather than the pair D-3 and D-5 to estimate $\frac{d\overline{\eta}}{dx}$ was that the PGF calculated using D-3 and D-5 (30 m separation) tended to be too noisy. Note that the sea level differences are on par with the stated accuracy of the pressure sensors (ca. 1 cm) but are still somewhat greater than the stated resolution of the sensors (0.2 mm).

Estimates of both the setup offset and C_D were found by trial and error iteration. To do this, we computed the lack of closure in the momentum balance, that is, the error E, as

$$E = PGF + BF - RSG \tag{15}$$

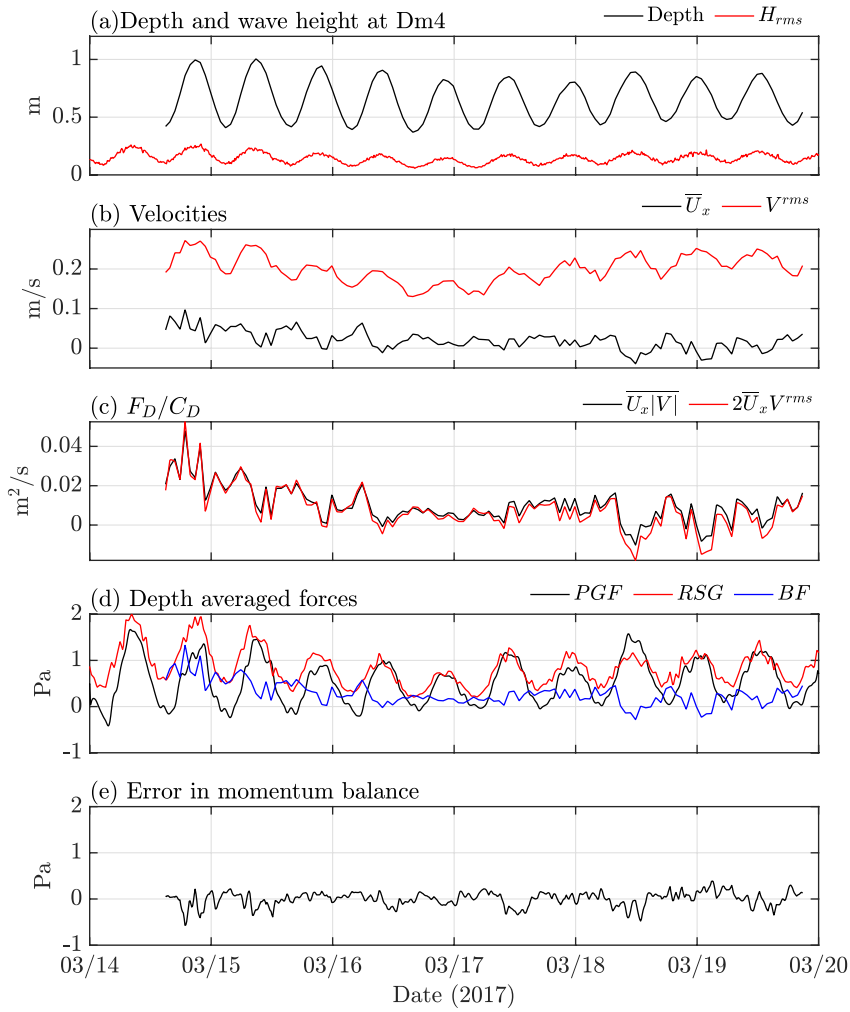

Figure 10. Reef flat dynamics: (a) Depth and rms wave height; (b) wave-averaged cross-reef flow and rms wave velocity; (c) drag/ρC_D: exact and the model of Wright and Thompson (1983); (d) forces on the reef flat—individual terms are defined in Equation 9; (e) error as given by Equation 15.

This iteration was carried out by first choosing a value of C_D and then finding the offset in the setup and C_D that produced a mean value of $E \simeq 0$. The iteration proceeded by choosing different values of C_D and repeating this process with the goal of making E_{rms} as small as possible and so that a linear fit of (PGF + D) as a function of (RSG + RF) should give a slope ≃1. Following this procedure, we found that the setup adjustment between D-2 and D-5 ≃ 7.6 mm upward and that $C_D \simeq 0.027$. The resulting force time series are shown in Figure 10. These parameters resulted in (PGF + D) = (0.97 ± 0.01)RSG ($r^2 = 0.83$) and gave a mean error of 0.0006 Pa and an rms error of 0.15 Pa (see Figure 10e). One key feature of the momentum balance is that waves on the reef flat were always important to the drag (Figure 10c), such that drag was well described by the linear model of Wright and Thompson (1983).

For the entire experiment (Figure 10d), at high tides, the *PGF* was directed *offshore* and nearly balanced the wave forcing (RSG), a behavior that is typically observed in surf zones on beaches (Longuet-Higgins & Stewart, 1964; Symonds et al., 1995), that is, from the standpoint of the momentum balance, the Ofu reef is closed at high tide. In contrast, at low tides, the wave forcing was primarily balanced by BF, a behavior characteristic of open reef systems, although in some cases (e.g., Hench et al., 2008), the wave forcing is unimportant and instead PGF ≃ BF. Thus, the Ofu reef behaves as either a closed or open system depending on the tidal water level. This behavior can be visualized using the force-balance "phase plane" shown in Lindhart et al. (2021). As seen in Figure 11, for water levels less than mean sea level, RSG tends to be ≃BF, although unlike what is seen in model results shown in Lindhart et al. (2021), the PGF contributes to the force balance even at the lowest water levels.

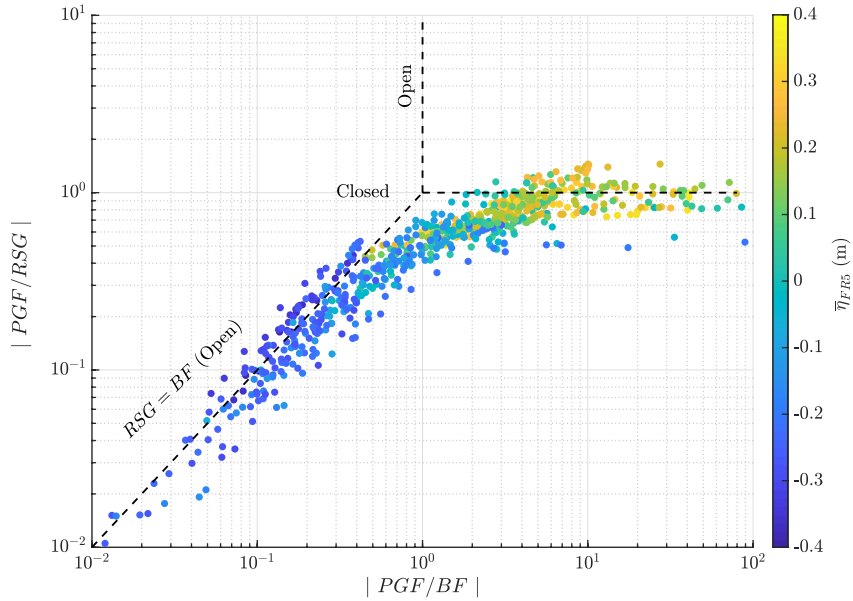

Figure 11. Reef flat dynamics: Force balances as a function of depth. The dashed lines indicate different regimes of the force balance defined by Equation 9.

For water levels somewhat greater than mean sea level, RSG ≃ PGF, although in this case, the BF still plays a small role in the force balance.

The value of C_D we found on the reef flat is an order of magnitude larger than what is typically found for smoother surfaces like sandy bottoms on the inner shelf, that is, ca. 0.0025 (Apotsos et al., 2008). This is plausible given the small-scale topography of the reef that varied between nearly flat to including corals that were ca. 10 cm high. This value of C_D is within the (wide) range of drag coefficients reported for reefs, which vary from 0.009 to 0.8 (Rosman & Hench, 2011). Using the law of the wall (Pope, 2000), Lentz et al. (2017) showed that, in some cases, variations in water depth could explain variability in C_D based on depth-averaged velocities. To test for this possibility, we considered an alternative to using a single value of C_D: Choose $C_D(t)$ so the momentum balance was satisfied for each time. Following this approach, we found no systematic variation of C_D with depth. Why this might be the case is that the observed velocity profiles (shown in 9) often cannot be described by the law of the wall, a likely effect of the vertical structure of the forcing. We tried using the near-bottom cross-reef velocity to parameterize drag, but doing so resulted in errors that were consistently larger than what was obtained using the depth-averaged velocity, and so are not presented here.

The stress we calculated by closing the momentum balance is somewhat different from that derived by Longuet-Higgins (2005) and used by Reniers et al. (2004) in the momentum balance in their model of surf zone flows. As argued by Longuet-Higgins (2005), the stress felt by the mean flow near the bottom but outside the wave boundary layer is

$$\tau_b = D/(\rho C) \tag{16}$$

where D is the rate of dissipation of wave energy, and C is the wave phase speed. For our case, a straightforward comparison of the quadratic stress model we used to that based on the wave dissipation derived by Longuet-Higgins (2005) (Figure 12) shows that the former (skill = 0.63; $r^2 = 0.68$) is a much better fit to what is required for the momentum balance than is the latter (skill = 0.2; $r^2 < 0$). This reflects the fact that there is an important difference between the Ofu reef flat flow and a beach: whereas net transport through the beach is 0, there is net onshore/offshore transport on the reef flat, transport that is determined by the dynamics of the entire reef flat/lagoon system (Lindhart et al., 2021; Monismith et al., 2013).

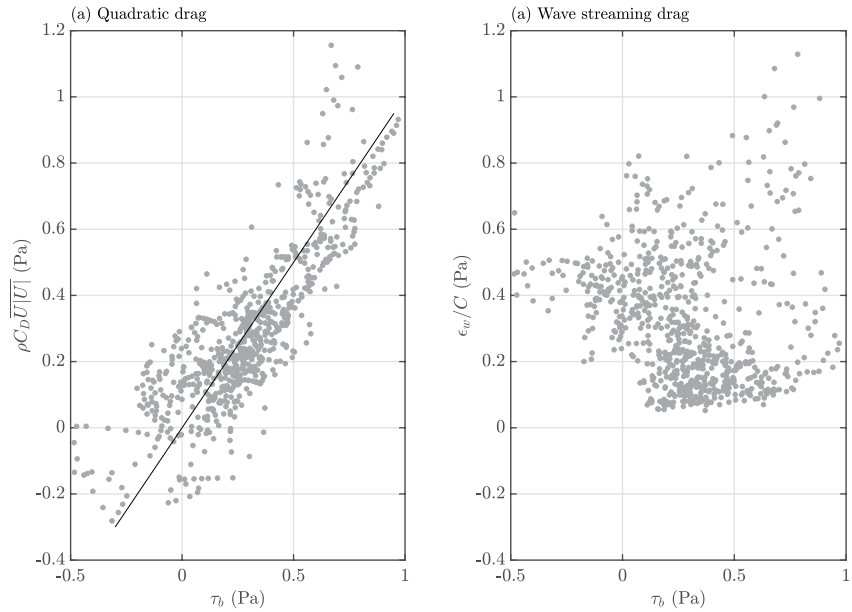

Figure 12. Estimates of bottom stress compared to bottom stress required to close the cross-reef momentum balance: (a) Quadratic drag as specified by Equation 13; (b) drag based on wave dissipation calculated using Equation 16.

5. Discussion and Conclusions

The Ofu reef appears to function as a (nearly) closed system at high tide, that is, the offshore-directed pressure gradient (PGF) balances the onshore-directed wave forcing (RSG), whereas at low tide, it appears open in that the wave forcing is balanced by bottom drag (BF). At high tide, the Ofu reef flat is similar to surf zones on beaches. In this case, the *offshore* direction of the PGF reflects the fact that as the depth on the reef flat increased with the tide, the strength of the wave forcing on the reef flat increased, although the wave-forced free-surface setup between the fore-reef and reef flat decreased. Nonetheless, at all times, the wave-driven setup in the lagoon and on the reef flat was nearly the same and so the cross-shore pressure gradient on the reef flat was always much smaller than the pressure gradient in the region near the reef crest where waves first break.

Waves on the reef flat were generally bore-like. Nonetheless, while standard parametrizations of breaking (e.g., Thornton and Guza, 1983) suggest that breaking was unimportant on the Ofu reef flat, visually, flows there often seemed highly turbulent and aerated, features expected of surf zones with breaking waves. Given that reef flats with broken waves are a common feature of reefs (Becker et al., 2014) and that flows there are important to wave runup and overtopping (Storlazzi et al., 2018), future efforts to examine this flow in more detail seem warranted.

Wave-driven flows through the Ofu reef system were also strongly modulated by the tides, with the strongest flows in the lagoon observed at high tides, although even for the lowest tides, there was flow through the system. In contrast, the situation on the reef flat at station D-4 was more complicated. First, the cross-shore wave transport was always onshore, whereas $\overline{q}_{x,E}$ recorded by the vADCP was directed onshore for part of the record and offshore for part of the record. Thus, the wave transport that we could only estimate rather than directly measure was crucial to sustaining onshore flows. Second, for higher tides, the principal direction of transport was directed nearly along the reef, rather than across the reef. This rotation is consistent with flow behavior seen in numerical simulations by Lowe et al. (2010) and Lindhart et al. (2021) for closed lagoon systems; it is not seen in open systems (e.g., John Brewer Reef—Symonds et al., 1995 or Moorea—Monismith et al., 2013). However, the presence of outflows on the reef flat near sta. H-1 (the vADCP data shown in Hefner et al. (2019)) suggests that for closed systems, shallow outflow channels may develop where the reef crest is locally lower than adjacent sections. Whether or not these depressions could ultimately develop into "full fledged" channels is an open question.

The vADCP allowed us to observe how the variation of wave forcing on the reef flat with water level affected the vertical structure of the flow on the reef flat: The velocity structure at high tide (Figures 9a–9c and 9g–9i)

resembled flows with undertows seen on beaches, most notably in the later part of the record where we observed net offshore flows at high tide. At low tide, the combined effects of the vertically variable wave forcing and the PGF both acting to force fluid onshore and the flow produce a strongly sheared unidirectional flow into the lagoon (Figures 9d–9f and 9j–9l). What is not clear from our observations is why the mean flow at D-4 shifted from onshore early in the experiment to offshore later. It appears that this behavior is similar to what happens in beach surf zones, that is, incident wave fields can force intense offshore-directed "rip" currents (Dalrymple et al., 2011). The development of rip currents has been seen in models of reef systems classed as closed, that is, those that are beach-like (Lindhart et al., 2021; Lowe et al., 2010).

Finally, one other feature of flows on reefs like the Ofu reef that deserves more consideration in future is the presence of relatively strong infragravity waves. Low-frequency variability of reef flat flows was comparable to swell-band variability, and water level fluctuations inside the lagoon showed the presence of multiple resonant modes, a behavior also seen on the reef flat on Ipan, which also appears to be "closed" (Péquignet et al., 2009). This is different from what was observed for flows and water levels on the much more open reef found on Moorea (Monismith et al., 2013), suggesting that active infragravity wave fields are also an important characteristic of closed systems.

Data Availability Statement

The original data discussed in this paper are available at the Stanford Digital Repository through the link: https://purl.stanford.edu/jv609mn4338.

Acknowledgments

The authors are grateful for support of this work by the National Science Foundation through grants OCE-1536502, OCE-1536618, OCE-1736668, and OCE-1948189. The authors also thank Pago Pago Marine Charters, Annie Adelson, and Emma Reid for their help with the 2017 field work, and Falk Feddersen and an anonymous reviewer for their most useful feedback. Finally, this work was conducted under permits from the U.S. Department of the Interior National Park Service, National Park of American Samoa, and the American Samoa Department of Marine and Wildlife Resources.

References

Apotsos, A., Raubenheimer, B., Elgar, S., & Guza, R. T. (2008). Wave-driven setup and alongshore flows observed onshore of a submarine canyon. *Journal of Geophysical Research*, *113*(C7), C07025. https://doi.org/10.1029/2007JC004514

Apotsos, A., Raubenheimer, B., Elgar, S., Guza, R. T., & Smith, J. A. (2007). Effects of wave rollers and bottom stress on wave setup. *Journal of Geophysical Research*, *112*(C2), C02003. https://doi.org/10.1029/2006JC003549

Becker, J. M., Merrifield, M. A., & Ford, M. (2014). Water level effects on breaking wave setup for Pacific island fringing reefs. *Journal of Geophysical Research: Oceans*, *119*(2), 914–932. https://doi.org/10.1002/2013JC009373

Callaghan, D. P., Nielsen, P., Cartwright, N., Gourlay, M. R., & Baldock, T. E. (2006). Atoll lagoon flushing forced by waves. *Coastal Engineering*, *53*(8), 691–704. https://doi.org/10.1016/j.coastaleng.2006.02.006

Chirayath, V., & Earle, S. A. (2016). Drones that see through waves–preliminary results from airborne fluid lensing for centimetre-scale aquatic conservation. *Aquatic Conservation: Marine and Freshwater Ecosystems*, *26*, 237–250. https://doi.org/10.1002/aqc.2654

Coronado, C., Candela, J., Iglesias-Prieto, R., Sheinbaum, J., López, M., & Ocampo-Torres, F. (2007). On the circulation in the puerto morelos fringing reef lagoon. *Coral Reefs*, *26*(1), 149–163. https://doi.org/10.1007/s00338-006-0175-9

Dalrymple, R. A., MacMahan, J. H., Reniers, A. J., & Nelko, V. (2011). Rip currents. *Annual Review of Fluid Mechanics*, *43*(1), 551–581. https://doi.org/10.1146/annurev-fluid-122109-160733

Davis, K., Lentz, S., Pineda, J., Farrar, J., Starczak, V., & Churchill, J. (2011). Observations of the thermal environment on red sea platform reefs: A heat budget analysis. *Coral Reefs*, *30*(1), 25–36. https://doi.org/10.1007/s00338-011-0740-8

Dean, R. G., & Dalrymple, R. A. (1991). *Water wave mechanics for engineers and scientists (Vol. 2)*. World Scientific Publishing Company.

Elgar, S., & Guza, R. T. (1985). Observations of bispectra of shoaling surface gravity waves. *Journal of Fluid Mechanics*, *161*(-1), 425–448. https://doi.org/10.1017/S0022112085003007

Feddersen, F., Guza, R., Elgar, S., & Herbers, T. (2000). Velocity moments in alongshore bottom stress parameterizations. *Journal of Geophysical Research*, *105*(C4), 8673–8686. https://doi.org/10.1029/2000jc900022

Gourlay, M. (1996). Wave set-up on coral reefs. 1. Set-up and wave-generated flow on an idealised two dimensional horizontal reef. *Coastal Engineering*, *27*(3–4), 161–193. https://doi.org/10.1016/0378-3839(96)00008-7

Grant, W. D., & Madsen, O. S. (1979). Combined wave and current interaction with a rough bottom. *Journal of Geophysical Research*, *84*(C4), 1797–1808. https://doi.org/10.1029/jc084ic04p01797

Hearn, C. J. (1999). Wave-breaking hydrodynamics within coral reef systems and the effect of changing relative sea level. *Journal of Geophysical Research*, *104*(C12), 30007–30019. https://doi.org/10.1029/1999jc900262

Hefner, J. S., Brian, B., Rogers Maticka, A. M. S. G., Samantha, A., & Woodson, C. B. (2019). Instrumentation for direct measurements of wave-driven flow over a fringing reef crest. *Limnology and Oceanography: Methods*, *17*(12), 627–638. https://doi.org/10.1002/lom3.10337

Hellerman, S. (1967). An updated estimate of the wind stress on the world ocean. *Monthly Weather Review*, *95*(9), 607–626. https://doi.org/10.1175/1520-0493(1967)095<0607:aueotw>2.3.co;2

Hench, J. L., Leichter, J. J., & Monismith, S. G. (2008). Episodic circulation and exchange in a wave-driven coral reef and lagoon system. *Limnology & Oceanography*, *53*(6), 2681–2694. https://doi.org/10.4319/lo.2008.53.6.2681

Henderson, S. M., Arnold, J., ñzkan Haller, H. T., & Solovitz, S. A. (2017). Depth dependence of nearshore currents and eddies. *Journal of Geophysical Research: Oceans*, *122*(11), 9004–9031. https://doi.org/10.1002/2016JC012349

Herdman, L. M., Hench, J. L., & Monismith, S. G. (2015). Heat balances and thermally driven lagoon-ocean exchangeson a tropical coral reef system (Moorea, French Polynesia). *Journal of Geophysical Research: Oceans*, *120*(2), 1233–1252. https://doi.org/10.1002/2014jc010145

Koweek, D. A., Dunbar, R. B., Monismith, S. G., Mucciarone, D. A., Woodson, C. B., & Samuel, L. (2015). High-resolution physical and biogeochemical variability from a shallow back reef on Ofu, American Samoa: An end-member perspective. *Coral Reefs*, *34*(3), 979–991. https://doi.org/10.1007/s00338-015-1308-9

Lentz, S. J., Churchill, J. H., Davis, K. A., & Farrar, J. T. (2016). Surface gravity wave transformation across a platform coral reef in the red sea. *Journal of Geophysical Research: Oceans*, *121*(1), 693–705. https://doi.org/10.1002/2015jc011142
Lentz, S. J., Davis, K. A., Churchill, J. H., & DeCarlo, T. M. (2017). Coral reef drag coefficients–water depth dependence. *Journal of Physical Oceanography*, *47*(5), 1061–1075. https://doi.org/10.1175/jpo-d-16-0248.1
Lindhart, M., Rogers, J. S., Maticka, S. A., Woodson, C. B., & Monismith, S. G. (2021). Wave modulation of flows on open and closed reefs. *Journal of Geophysical Research: Oceans*, *126*(4), e2020JC016645. https://doi.org/10.1029/2020JC016645
Longuet-Higgins, M. (2005). On wave set-up in shoaling water with a rough sea bed. *Journal of Fluid Mechanics*, *527*, 217–234. https://doi.org/10.1017/S0022112004003222
Longuet-Higgins, M., & Stewart, R. (1964). Radiation stresses in water waves; A physical discussion, with applications. *Deep-Sea Research and Oceanographic Abstracts*, *11*(4), 529–562. https://doi.org/10.1016/0011-7471(64)90001-4
Lowe, R. J., Falter, J. L., Monismith, S. G., & Atkinson, M. J. (2009). Wave-driven circulation of a coastal reef–lagoon system. *Journal of Physical Oceanography*, *39*(4), 873–893. https://doi.org/10.1175/2008jpo3958.1
Lowe, R. J., Hart, C., & Pattiaratchi, C. B. (2010). Morphological constraints to wave-driven circulation in coastal reef-lagoon systems: A numerical study. *Journal of Geophysical Research*, *115*(C9), C09021. https://doi.org/10.1029/2009jc005753
MacMahan, J. H., Thornton, E. B., & Reniers, A. J. (2006). Rip current review. *Coastal Engineering*, *53*(2–3), 191–208. https://doi.org/10.1016/j.coastaleng.2005.10.009
Martins, K., Blenkinsopp, C. E., Deigaard, R., & Power, H. E. (2018). Energy dissipation in the inner surf zone: New insights from lidar-based roller geometry measurements. *Journal of Geophysical Research: Oceans*, *123*(5), 3386–3407. https://doi.org/10.1029/2017JC013369
Maticka, S. (2019). *A tale of two reefs: Hydrodynamics of a fringing reef and a reef atoll (Unpublished doctoral dissertation)*. Stanford University.
Mei, C. C., Stiassnie, M., & Yue, D. K.-P. (1989). *Theory and applications of ocean surface waves: Part 1: Linear aspects part 2: Nonlinear aspects*. World Scientific.
Monismith, S. G., Herdman, L. M., Ahmerkamp, S., & Hench, J. L. (2013). Wave transformation and wave-driven flow across a steep coral reef. *Journal of Physical Oceanography*, *43*(7), 1356–1379. https://doi.org/10.1175/jpo-d-12-0164.1
Monismith, S. G., Rogers, J. S., Koweek, D., & Dunbar, R. B. (2015). Frictional wave dissipation on a remarkably rough reef. *Geophysical Research Letters*, *42*(10), 4063–4071. https://doi.org/10.1002/2015gl063804
Munk, W. H., & Sargent, M. C. (1954). Adjustment of bikini atoll to ocean waves. *Eos, Transactions American Geophysical Union*, *29*(6), 855–860. https://doi.org/10.1029/tr029i006p00855
Oliver, T. A., & Palumbi, S. R. (2009). Distributions of stress-resistant coral symbionts match environmental patterns at local but not regional scales. *Marine Ecology Progress Series*, *378*, 93–103. https://doi.org/10.3354/meps07871
Péquignet, A.-C. N., Becker, J. M., Merrifield, M. A., & Aucan, J. (2009). Forcing of resonant modes on a fringing reef during tropical storm man-yi. *Geophysical Research Letters*, *36*(3). https://doi.org/10.1029/2008gl036259
Pope, S. B. (2000). *Turbulent flows*. Cambridge University Press.
Raubenheimer, B., Guza, R., & Elgar, S. (1996). Wave transformation across the inner surf zone. *Journal of Geophysical Research*, *101*(C11), 25589–25597. https://doi.org/10.1029/96jc02433
Raubenheimer, B., Guza, R. T., Elgar, S., & Kobayashi, N. (1995). Swash on a gently sloping beach. *Journal of Geophysical Research: Oceans*, *100*(C5), 8751–8760. https://doi.org/10.1029/95JC00232
Reniers, A., Thornton, E., Stanton, T., & Roelvink, D. (2004). Vertical flow structure during sandy duck: Observations and modeling. *Coastal Engineering*, *51*(3), 237–260. https://doi.org/10.1016/j.coastaleng.2004.02.001
Roelvink, D. (1993). Dissipation in random wave groups incident on a beach. *Coastal Engineering*, *19*(1), 127–150. https://doi.org/10.1016/0378-3839(93)90021-Y
Roelvink, D., & Reniers, A. (2011). *A guide to modeling coastal morphology* (Vol.12). World Scientific Publishing Company.
Rogers, J. S., Maticka, S. A., Chirayath, V., Woodson, C. B., Alonso, J. J., & Monismith, S. G. (2018). Connecting flow over complex terrain to hydrodynamic roughness on a coral reef. *Journal of Physical Oceanography*, *48*(2018), 1567–1587. https://doi.org/10.1175/jpo-d-18-0013.1
Rogers, J. S., Monismith, S. G., Fringer, O. B., Koweek, D. A., & Dunbar, R. B. (2017). A coupled wave-hydrodynamic model of an atoll with high friction: Mechanisms for flow, connectivity, and ecological implications. *Ocean Modelling*, *110*, 66–82. https://doi.org/10.1016/j.ocemod.2016.12.012
Rosman, J. H., & Hench, J. L. (2011). A framework for understanding drag parameterizations for coral reefs. *Journal of Geophysical Research*, *116*(C8), C08025. https://doi.org/10.1029/2010jc006892
Ruessink, B. G., Miles, J. R., Feddersen, F., Guza, R. T., & Elgar, S. (2001). Modeling the alongshore current on barred beaches. *Journal of Geophysical Research*, *106*(C10), 22451–22463. https://doi.org/10.1029/2000JC000766
Sheremet, A., Guza, R., Elgar, S., & Herbers, T. (2002). Observations of nearshore infragravity waves: Seaward and shoreward propagating components. *Journal of Geophysical Research*, *107*(C8), 10–11. https://doi.org/10.1029/2001jc000970
Sous, D., Dodet, G., Bouchette, F., & Tissier, M. (2020). Momentum balance over a barrier reef. *Journal of Geophysical Research: Oceans*, *125*(2). e2019JC015503. https://doi.org/10.1029/2019jc015503
Storlazzi, C. D., Gingerich, S. B., van Dongeren, A., Cheriton, O. M., Swarzenski, P. W., Quataert, E., et al. (2018). Most atolls will be uninhabitable by the mid-21st century because of sea-level rise exacerbating wave-driven flooding. *Science Advances*, *4*(4), eaap9741. https://doi.org/10.1126/sciadv.aap9741
Svendsen, I. A. (1984). Mass flux and undertow in a surf zone. *Coastal Engineering*, *8*(4), 347–365. https://doi.org/10.1016/0378-3839(84)90030-9
Symonds, G., Black, K. P., & Young, I. R. (1995). Wave-driven flow over shallow reefs. *Journal of Geophysical Research*, *100*(C2), 2639–2648. https://doi.org/10.1029/94jc02736
Taebi, S., Lowe, R. J., Pattiaratchi, C. B., Ivey, G. N., Symonds, G., & Brinkman, R. (2011). Nearshore circulation in a tropical fringing reef system. *Journal of Geophysical Research*, *116*(C2), C02016. https://doi.org/10.1029/2010jc006439
Thornton, E. B., & Guza, R. (1983). Transformation of wave height distribution. *Journal of Geophysical Research*, *88*(C10), 5925–5938. https://doi.org/10.1029/jc088ic10p05925
Vetter, O., Becker, J. M., Merrifield, M. A., Pequignet, A.-C. N., Aucan, J., Boc, S. J., & Pollock, C. E. (2010). Wave setup over a Pacific island fringing reef. *Journal of Geophysical Research*, *115*(C12), C12066. https://doi.org/10.1029/2010JC006455
Wiens, H. J., et al. (1962). *Atoll environment and ecology*. Yale University Press.
Willmott, C. J. (1981). On the validation of models. *Physical Geography*, *2*(2), 184–194. https://doi.org/10.1080/02723646.1981.10642213
Wright, D. G., & Thompson, K. R. (1983). Time-averaged forms of the nonlinear stress law. *Journal of Physical Oceanography*, *13*(2), 341–345. https://doi.org/10.1175/1520-0485(1983)013<0341:tafotn>2.0.co;2
Yao, Y., Huang, Z., Monismith, S. G., & Lo, E. Y. (2012). 1dh boussinesq modeling of wave transformation over fringing reefs. *Ocean Engineering*, *47*, 30–42. https://doi.org/10.1016/j.oceaneng.2012.03.010

Zhang, Z., Falter, J., Lowe, R., & Ivey, G. (2012). The combined influence of hydrodynamic forcing and calcification on the spatial distribution of alkalinity in a coral reef system. *Journal of Geophysical Research*, *117*(C4), C04034. https://doi.org/10.1029/2011jc007603

Zhang, Z., Falter, J., Lowe, R., Ivey, G., & McCulloch, M. (2013). Atmospheric forcing intensifies the effects of Regional Ocean warming on reef-scale temperature anomalies during a coral bleaching event. *Journal of Geophysical Research: Oceans*, *118*(9), 4600–4616. https://doi.org/10.1002/jgrc.20338